Patterns of thermomagnetic convection in magnetic fluids subjected to spatially modulated magnetic fields

Adrian Lange* and Stefan Odenbach
TU Dresden, Institute of Fluid Mechanics, Chair of Magnetofluiddynamics, DE-01062 Dresden, Germany
(Received 3 March 2011; published 10 June 2011)

An analysis of thermomagnetic convection in a thin horizontal layer of magnetic fluid constrained horizontally by impermeable layers and subjected to a spatially and symmetrically modulated magnetic field is presented. The magnetic field as well as the temperature gradient are oriented vertically. For any nonzero magnetic field the base state is a convective one formed by a double vortex which reflects the symmetrical modulation. For long wave modulations the linear stability analysis reveals that the critical Rayleigh number Ra_c for the stability of the base state against small disturbances increases with increasing magnetic driving force. An analytical expression for Ra_c is derived which shows the characteristic feature of sudden jumps of Ra_c at particular values of the magnetic driving force.

DOI: 10.1103/PhysRevE.83.066305 PACS number(s): 47.65.Cb, 47.20.−k, 44.27.+g

I. INTRODUCTION

Fluidic systems which are driven out of equilibrium by the temperature dependence of the density of the fluid have been long studied with respect to the emerging patterns and their stability and belong now to the set of classical pattern forming systems [1,2]. By using a magnetic fluid (MF), also called a ferrofluid, as the working substance instead of classical fluids such as ethanol [3], CO_2 gas [4,5], or liquid normal ^{4}He [6], additionally ways open up to generate patterns. Magnetic fluids—stable colloidal suspensions of ferromagnetic nanoparticles (typically magnetite or cobalt) dispersed in a carrier liquid (typically oil or water)—are superparamagnetic fluids. Their magnetization generates a magnetic force in a complex interaction with an applied magnetic field of moderate strength. That force can drive the system out of equilibrium, too. Thus, in a horizontal layer of MF subjected to a vertical gradient of temperature and a vertical magnetic field, convection can be initiated in two different ways.

Besides density-driven convection, the temperature-dependent magnetization, whose gradient is antiparallel to the temperature gradient, is the other cause for triggering convective motion. As a consequence of the gradient of magnetization ∇M, the inner magnetic field within the fluid has also a gradient being antiparallel to ∇M. If now a fluid element with magnetization M is adiabatically moved from the hot bottom to the cold top of the layer, where the magnetization $M - \Delta M$ is present, a difference in the magnetization between the fluid element and the surrounding fluid exists. This difference interacts with the gradient of the inner field to a resulting magnetic force, which points in the same direction as the initial adiabatic movement [7]. Thus the magnetic force can generate a destabilization of the fluid layer which leads to a convective motion, called thermomagnetic convection. The strength of the force is controlled by the strength of the magnetic field.

The phenomenon of thermomagnetic convection is well studied in the case of static external magnetic fields [8–10]. Special attention was paid to the interaction of the thermomagnetic convection with the density driven one [8]. The resulting flow patterns of aligned as well as hexagonal and irregularly oriented convection rolls were visualized in [9,10]. Also the limits of stability and the critical wave number were determined experimentally [11] and later theoretically confirmed [12].

Widening the focus of interest, the first modulations of the magnetic field were made with respect to time and led to parametrically driven convection [7]. For this type of excitation it was found that the critical temperature difference for the onset of convection is frequency dependent. A drawback of this type of excitation is that frequencies of the magnetic field above 5 Hz are difficult to implement. Thus the prospects of variable stimulation are limited.

Therefore the idea of a spatially modulated field appeals. Such a modulation is easy to accomplish by placing, for instance, sinus-shaped iron bars in a constant magnetic field. A sketch of such an arrangement is shown in Fig. 1 for the case of an asymmetrical modulation by a bar beneath the ferrofluid layer. With such a way of implementation, several different types of spatial modulations are possible. One can use one or two bars, the bars may have the same or a different wavelength, or even a phase shift between both modulations is possible. Of these different types, here one generic spatial modulation is chosen and studied in detail.

The direction of this work is to determine the base state and its stability by a linear analysis in a layer of magnetic fluid which is subjected to a spatial symmetrical modulation of the magnetic field. The paper is therefore organized as follows. Numerical calculations and an analytical approximation of the modulated field is presented in Sec. II. The governing equations of the considered system are presented in Sec. III A. In Sec. III B the base state is determined, followed by a linear analysis of its stability in Sec. III C. The results of that analysis as well as the discussion of the results make up the content of Sec. IV. Section V contains concluding remarks.

*adrian.lange@tu-dresden.de

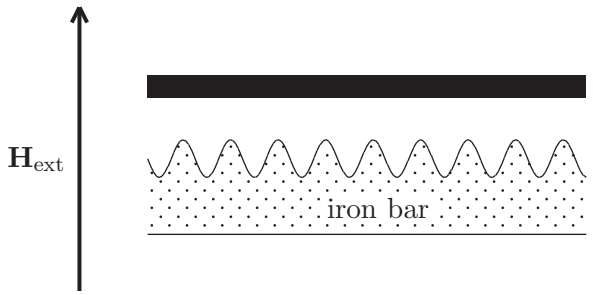

FIG. 1. Sketch of an asymmetric modulation of a constant external magnetic field $\mathbf{H}_{\text{ext}}$ by one iron bar beneath a ferrofluid layer (black filled rectangle).

II. MAGNETIC FIELD

According to the aim of the work, we concentrate on the symmetrical modulation of an external magnetic field by two iron bars placed beneath and above a ferrofluid layer with a chosen thickness of $d = 2$ mm. For further systematic analysis it is of immediate importance to address an analytical description of the magnetic fields inside and outside the ferrofluid layer. Since to the best of our knowledge no analytical solution is known, the problem is numerically tackled and that solution approximated afterward. Figure 2 shows the central part of the setup for the two-dimensional numerical simulation because the setup will be lateral invariant in the y direction. With the assumption that the magnetization $\mathbf{M}$ of the magnetic fluid depends linearly on the applied magnetic field $\mathbf{H}$, $\mathbf{M} = (\mu_r - 1)\mathbf{H}$, the magnetic induction is given by $\mathbf{B} = \mu_0 (\mathbf{M} + \mathbf{H}) = \mu_0 \mu_r \mathbf{H}$. The relative permeability of the MF is denoted by μ_r, and μ_0 is the permeability of free space. The permeabilities are $\mu_r = 1.2$ for the MF and $\mu_r = 4000$ for iron, the wavelength of the sinus-shaped iron bar is $\lambda \simeq 3.14$ cm, its thickness averages to 1.16 cm, and the amplitude of the sinusoidal part is $\simeq 1.25$ mm. This setup is subjected to a vertical magnetic induction of 1 T.

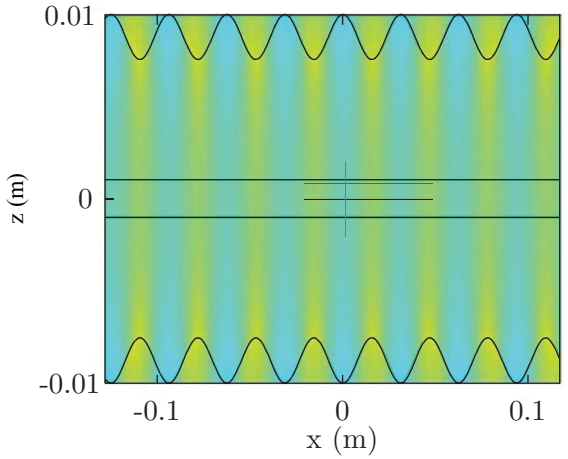

FIG. 2. (Color online) Symmetric arrangement of two sinus-shaped iron bars (gray, $\lambda \simeq 3.14$ cm) beneath and above a centered ferrofluid layer (black). The white area indicates air.

The calculations were performed by COMSOL Multiphysics® on a triangular grid with nearly 1 44 000 elements. The ferrofluid layer and the bars with a horizontal extension between $x = -0.16$ m and $x = 0.16$ m are centrally placed in a computational region with a lateral length of 0.5 m. At all boundaries of the computational region, a vertical induction of 1 T was imposed, thus the entire setup of ferrofluid layer and iron bars is imbedded in a vertically oriented, constant external magnetic induction.

Figure 3 presents the color-coded numerical values of B_z in the area between the two sinus-shaped boundaries of the iron bars. In the middle of the graph, the ferrofluid layer is indicated by two long horizontal black lines. The spatial modulations are clearly visible between the high [yellow (light gray)] and low [turquoise (dark gray)] values of B_z. To study this modulation in more detail, the short black (lower) and red (upper) horizontal lines at $z = 0$ and $z = 0.8$ mm, respectively, as well as the purple (vertical) line at $x = 1.4$ mm indicate the range from which data were collected for further inspection, particularly for a comparison with an analytical approximation.

For that purpose, it is advantageous to introduce dimensionless quantities (indicated by a bar): the components of the magnetic induction are scaled with the mean value of $B_z(x)$ at $z = 0$, $B_{z,\text{mean}}(x) \simeq 1.13$ T, and all lengths with d. The black [red (dark gray)] line in Figs. 4(a) and 4(b) shows the excellent sinus-like variation of $\bar{B}_z(\bar{x})$ at $z = 0$ [$z = 0.8$ mm], i.e., across the entire thickness of the layer. As can be seen in Fig. 4(a), both lines overlap so well which means that $\bar{B}_z$ is nearly constant over the width of the layer, see also Fig. 4(c). The variation is less than 0.2 %. In contrast to the strength of $\bar{B}_z(\bar{x})$, $\bar{B}_x(\bar{x})$ is about two orders of magnitude smaller, compare Figs. 4(a) and 4(c) with Figs. 4(b) and 4(d), respectively. Thus a nearly perfect vertical and oscillating magnetic field is generated.

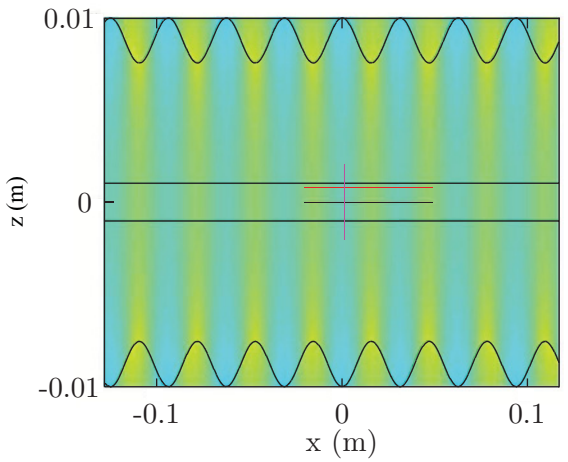

FIG. 3. (Color online) Plot of the z component of $\mathbf{B}$ for a symmetrical modulation of the magnetic field by iron bars (indicated at the top and bottom of the graph, see also Fig. 2). Yellow (light gray) [turquoise (dark gray)] indicates a high [low] value of B_z. The short black (lower) and red (upper) horizontal lines inside the layer at $z = 0$ ($z = 0.8$ mm) indicate the range of data for Figs. 4 (a) and 4(b); the purple (vertical) line at $x = 1.4$ mm the range of data for Figs. 4 (c) and 4(d).

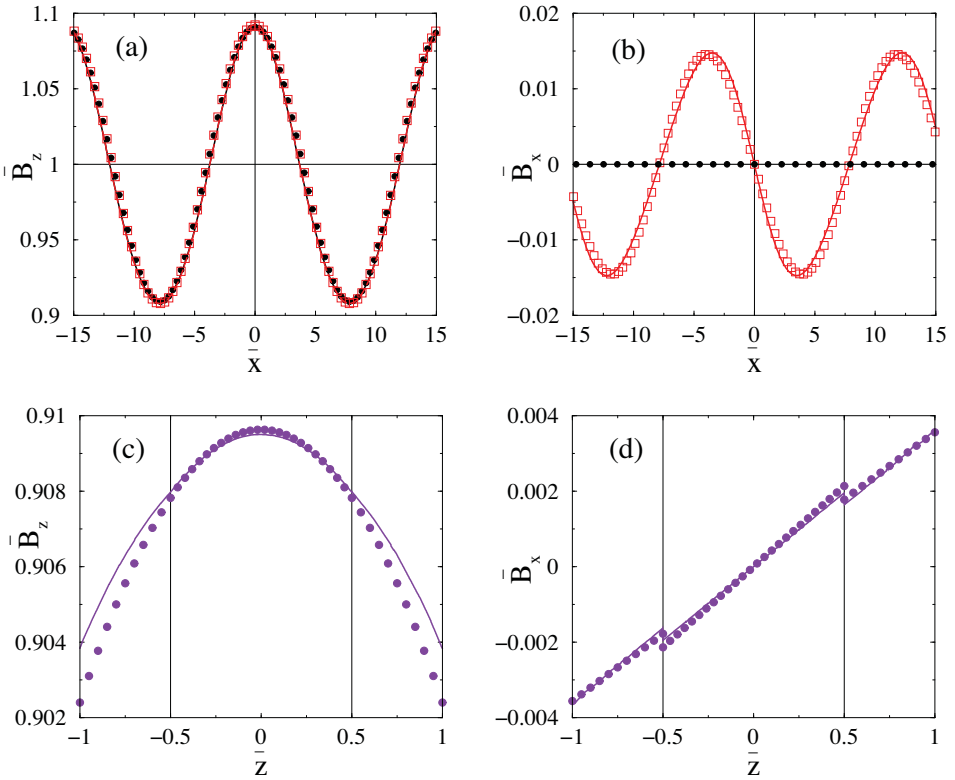

FIG. 4. (Color online) Plot of $\bar{B}_z$ (a) and $\bar{B}_x$ (b) at $z = 0$ (black) and $z = 0.8$ mm [red (gray)] vs the horizontal coordinate $\bar{x}$ with $\bar{x} = x/d - 8.26$ for $-1.35 \leqslant x \leqslant 4.65$ cm. The lines show the results of the numerical evaluation, the symbols the analytical approximation. The excellent sinusoidal variation across the layer can be seen from graph (a), where a comparison of the order of magnitude between (a) and (b) reveals that the field is nearly perfectly vertically oriented. Graphs (c) and (d) are plots of $\bar{B}_z$ (c) and $\bar{B}_x$ (d) at $x = 1.4$ mm [purple (gray)] vs the vertical coordinate $\bar{z}$ and indicate that both components are almost constant across the fluid layer bounded at $\bar{z} = \pm 0.5$.

For an analytical approximation, the dependence with respect to $\bar{x}$ is modeled by trigonometric functions and with respect to $\bar{z}$ with terms which are in maximum quadratic in $\bar{z}$,

$$\bar{B}_x = \sin(\bar{k}\bar{x})\,(\mathcal{B}\bar{z}), \tag{2.1}$$

$$\bar{B}_z = 1 + \cos(\bar{k}\bar{x})(E + G\bar{z}^2)\,, \tag{2.2}$$

with

$$\bar{k} = \frac{2\pi d}{\lambda}, \quad \mathcal{B} = -\bar{k}E, \quad G = \frac{\bar{k}^2 E}{2}. \tag{2.3}$$

The dimensionless wave number is denoted by $\bar{k}$ and two of the three constants in Eqs. (2.1) and (2.2) were determined by the condition that the divergence as well as the vorticity of B is zero and by the assumption that $G\bar{z}^2 \ll E$ holds. The third, E, is a fit parameter which yields for $E = 0.091$ a very good agreement for components in both the $\bar{x}$ and $\bar{z}$ directions, as the symbols in Fig. 4 show.

III. SYSTEM

A. Basic equations

A laterally infinite horizontal layer of an incompressible layer of magnetic fluid (density ρ, dynamic viscosity η) of thickness d in the x-y plane is bounded by two rigid impermeable boundaries in the planes $z = \pm d/2$. The setup is heated from below with a temperature of T_b for the bottom impermeable boundary which results in a temperature difference of $\delta T = T_b - T_t$ with respect to the top impermeable boundary with the temperature $T_t < T_b$. The layer is sandwiched between two sinus-shaped iron bars, see Fig. 2, and the entire system is subjected to a constant external magnetic field $\mathbf{H}_{\text{ext}} = (0,0,H_{\text{ext}})$. The system is governed by the equation of continuity

$$\operatorname{div} \mathbf{v} = 0, \tag{3.1}$$

the Navier-Stokes equation in the Boussinesq approximation,

$$\rho_0 \left[\frac{\partial \mathbf{v}}{\partial t} + (\mathbf{v}\,\operatorname{grad})\,\mathbf{v}\right] = -\operatorname{grad} p + \rho\,\mathbf{g} + \mu_0\,(\mathbf{M}\,\operatorname{grad})\,\mathbf{H} + \eta\,\Delta\mathbf{v}, \tag{3.2}$$

and the equation of heat conduction,

$$\frac{\partial T}{\partial t} + (\mathbf{v}\,\operatorname{grad})\,T = \kappa\,\Delta T. \tag{3.3}$$

The density at the mean temperature $T_0 = (T_b + T_t)/2$ is denoted by ρ_0, the thermal diffusivity by κ, and the acceleration due to gravity by $\mathbf{g} = (0,0,-g)$ and a linear dependence of the density on the temperature is assumed, $\rho = \rho_0\,[1 - \alpha\,(T - T_0)]$, where α is the thermal expansion coefficient.

Since we assume that the system is laterally invariant in the y direction, only the x and z components are considered. It leads to the following dimensionless equations for the corresponding components of $\mathbf{v} = (u,0,w)$ and the temperature T:

$$\frac{\partial \bar{u}}{\partial \bar{x}} + \frac{\partial \bar{w}}{\partial \bar{z}} = 0, \tag{3.4}$$

$$\frac{1}{\mathrm{Pr}}\left[\frac{\partial \bar{u}}{\partial \bar{t}}+\left(\bar{u}\frac{\partial}{\partial \bar{x}}+\bar{w}\frac{\partial}{\partial \bar{z}}\right)\bar{u}\right]=-\frac{\partial \bar{p}}{\partial \bar{x}}+\Delta\bar{u}+\frac{\mathrm{Ra}_m(\mu_r-1)E\bar{k}\sin(\bar{k}\bar{x})[E\cos(\bar{k}\bar{x})(\bar{k}^2\bar{z}^2-2)-2]}{2\mu_r^2}, \tag{3.5}$$

$$\frac{1}{\mathrm{Pr}}\left[\frac{\partial \bar{w}}{\partial \bar{t}}+\left(\bar{u}\frac{\partial}{\partial \bar{x}}+\bar{w}\frac{\partial}{\partial \bar{z}}\right)\bar{w}\right]=-\frac{\partial \bar{p}}{\partial \bar{z}}+\Delta\bar{w}+\frac{\mathrm{Ra}_m(\mu_r-1)E\bar{k}^2\bar{z}[E(2+\bar{k}^2\bar{z}^2)+2\cos(\bar{k}\bar{x})]}{2\mu_r^2}+\mathrm{Ra}(\bar{T}-\bar{T}_0)-\frac{\rho_0 g d^3}{\kappa\eta}, \tag{3.6}$$

$$\frac{\partial \bar{T}}{\partial \bar{t}}+\left(\bar{u}\frac{\partial}{\partial \bar{x}}+\bar{w}\frac{\partial}{\partial \bar{z}}\right)\bar{T}=\Delta\bar{T}. \tag{3.7}$$

The Prandtl number $\mathrm{Pr}=\eta/(\rho_0\kappa)$ characterizes the fluid, where the Rayleigh number,

$$\mathrm{Ra}=\frac{g\rho_0\alpha\delta T d^3}{\kappa\,\eta}, \tag{3.8}$$

and its magnetic counterpart [7],

$$\mathrm{Ra}_m=\frac{\mu_0 K^2\delta T^2 d^2}{\kappa\,\eta}, \tag{3.9}$$

relate the destabilizing effects of buoyancy and magnetic force, respectively, to the stabilizing effects of viscous friction and head conduction. The velocity was scaled with κ/d, the time with d^2/κ, the temperature with δT, the pressure with $(\kappa\,\eta)/d^2$, and the magnetic field with $K\delta T$, where $K=-(\partial M/\partial T)_H$ is the pyromagnetic coefficient. After the scaling of **H** and **M**, the corresponding dimensionless expressions which follow from Eqs. (2.1) and (2.2) were used for Eqs. (3.5) and (3.6). As a first step of a systematic analysis, a solution describing the base state is searched for where realistic material parameters are taken into account.

B. Base state

Since the Prandtl number of real magnetic fluids is large compared to 1 [13,14], the left-hand side of Eqs. (3.5) and (3.6) is set to zero. As the base state is a stationary one, a solution has to be determined for the equations

$$0=-\frac{\partial \bar{p}}{\partial \bar{x}}+\Delta\bar{u}+\mathrm{Ra}_m(\mu_r-1)E\bar{k}\sin(\bar{k}\bar{x})\times\frac{[E\cos(\bar{k}\bar{x})(\bar{k}^2\bar{z}^2-2)-2]}{2\mu_r^2}, \tag{3.10}$$

$$0=-\frac{\partial \bar{p}}{\partial \bar{z}}+\Delta\bar{w}+\mathrm{Ra}(\bar{T}-\bar{T}_0)-\frac{\rho_0 g d^3}{\kappa\eta}+\frac{\mathrm{Ra}_m(\mu_r-1)E\bar{k}^2\bar{z}[E(2+\bar{k}^2\bar{z}^2)+2\cos(\bar{k}\bar{x})]}{2\mu_r^2}, \tag{3.11}$$

$$0=-\left(\bar{u}\frac{\partial}{\partial \bar{x}}+\bar{w}\frac{\partial}{\partial \bar{z}}\right)\bar{T}+\Delta\bar{T}, \tag{3.12}$$

augmented by Eq. (3.4). This set of equations has to be supplemented by rigid boundary conditions for the velocity,

$$\bar{u}=\bar{w}=0 \quad \text{at } \bar{z}=\pm 1/2, \tag{3.13}$$

and a constant temperature at the bottom and upper boundary, respectively,

$$\bar{T}=\bar{T}_t \quad \text{at } \bar{z}=1/2,$$
$$\bar{T}=\bar{T}_b \quad \text{at } \bar{z}=-1/2. \tag{3.14}$$

By restricting the analysis to modulations with a long wavelength, $k\,d\ll 1$, a perturbational ansatz of the kind

$$\begin{aligned}\bar{X}(\bar{x},\bar{z})=&\,\overline{X^0}(\bar{z})+\bar{k}\overline{X^1}(\bar{z})+\cdots+\bar{k}^4\overline{X^4}(\bar{z})\\&+\cos(\bar{k}\bar{x})\left[\overline{X_k^0}(\bar{z})+\bar{k}\overline{X_k^1}(\bar{z})+\cdots+\bar{k}^4\overline{X_k^4}(\bar{z})\right]\\&+\cos(2\bar{k}\bar{x})\left[\overline{X_{2k}^0}(\bar{z})+\bar{k}\overline{X_{2k}^1}(\bar{z})+\cdots+\bar{k}^4\overline{X_{2k}^4}(\bar{z})\right]\\&+O(\bar{k}^5)\end{aligned} \tag{3.15}$$

can be employed, where $\bar{X}$ stands for $\bar{u}$, $\bar{w}$, $\bar{T}$, and $\bar{p}$. For $\bar{u}$ the cosine functions have to be substituted by the corresponding sine functions. The trigonometric functions with the double argument are caused by the particular form of the magnetic force term in Eq. (3.10).

Inserting the ansatz (3.15) into Eqs. (3.4), (3.10)–(3.14), a hierarchy of equations follows sorted by the power of $\bar{k}$ and all possible combinations of the employed trigonometric functions. The principal way to determine the solution is exemplarily shown in the lowest order of $\bar{k}$.

At the orders $O[\bar{k}^0\sin(\bar{k}\bar{x})]$, $O[\bar{k}^0\sin(2\bar{k}\bar{x})]$ from Eqs. (3.10) and (3.13) and at the orders $O[\bar{k}^0\cos(\bar{k}\bar{x})]$ and $O[\bar{k}^0\cos(2\bar{k}\bar{x})]$ from Eqs. (3.4) and (3.13) one get

$$\frac{\partial^2\overline{u_k^0}}{\partial\bar{z}^2}=0 \qquad \overline{u_k^0}(1/2)=\overline{u_k^0}(-1/2)=0, \tag{3.16}$$

$$\frac{\partial^2\overline{u_{2k}^0}}{\partial\bar{z}^2}=0 \qquad \overline{u_{2k}^0}(1/2)=\overline{u_{2k}^0}(-1/2)=0, \tag{3.17}$$

$$\frac{\partial^2\overline{w_k^0}}{\partial\bar{z}^2}=0 \qquad \overline{w_k^0}(1/2)=\overline{w_k^0}(-1/2)=0, \tag{3.18}$$

$$\frac{\partial^2\overline{w_{2k}^0}}{\partial\bar{z}^2}=0 \qquad \overline{w_{2k}^0}(1/2)=\overline{w_{2k}^0}(-1/2)=0, \tag{3.19}$$

with the solution $\overline{u_k^0}=\overline{u_{2k}^0}=\overline{w_k^0}=\overline{w_{2k}^0}=0$. At the order $O(\bar{k}^0)$ in Eqs. (3.4) and (3.10)–(3.14), the classical Rayleigh-Bénard problem is recovered with its solution of a quiescent fluid in a vertical temperature gradient,

$$\overline{u^0}=\overline{w^0}=0, \tag{3.20}$$

$$\overline{T^0}=\bar{T}_0-\bar{z}. \tag{3.21}$$

With this partial solution, the orders $O[\bar{k}^0\cos(\bar{k}\bar{x})]$ and $O[\bar{k}^0\cos(2\bar{k}\bar{x})]$ from Eqs. (3.12) and (3.14) yield

$$\frac{\partial^2\overline{T_k^0}}{\partial\bar{z}^2}=0, \qquad \overline{T_k^0}(1/2)=\overline{T_k^0}(-1/2)=0, \quad (3.22)$$

$$\frac{\partial^2\overline{T_{2k}^0}}{\partial\bar{z}^2}=0, \qquad \overline{T_{2k}^0}(1/2)=\overline{T_2^0k}(-1/2)=0. \quad (3.23)$$

Solving this set of equations generates the remaining solution, $\overline{T_k^0}=\overline{T_{2k}^0}=0$.

Repeating that procedure up to $O(\bar{k}^4)$, the base state is finally given by

$$\bar{u}_b(\bar{x},\bar{z})=-\left[\sin(\bar{k}\bar{x})+\frac{E}{2}\sin(2\bar{k}\bar{x})\right]\mathrm{Ra}_m E(\mu_r-1)\times\frac{(4\bar{z}^2-1)(20\bar{z}^2-1)\bar{k}^3}{1920\mu_r^2}, \quad (3.24)$$

$$\bar{w}_b(\bar{x},\bar{z})=[\cos(\bar{k}\bar{x})+E\cos(2\bar{k}\bar{x})]\,\mathrm{Ra}_m E(\mu_r-1)\times\frac{\bar{z}(4\bar{z}^2-1)^2\bar{k}^4}{1920\mu_r^2}, \quad (3.25)$$

$$\bar{T}_b(\bar{x},\bar{z})=\bar{T}_0-\bar{z}-[\cos(\bar{k}\bar{x})+E\cos(2\bar{k}\bar{x})]\,\mathrm{Ra}_m E\times\frac{(\mu_r-1)\bar{z}(4\bar{z}^2-1)[16\bar{z}^2(5\bar{z}^2-4)+19]\bar{k}^4}{1612800\mu_r^2}. \quad (3.26)$$

For a vanishing magnetic Rayleigh number, i.e., for a vanishing external magnetic field, the motionless base state with a linear temperature profile inside the layer is recovered. If the spatially modulated magnetic field is turned on, the temperature field is modified. But the real qualitatively different feature compared to the classical Rayleigh-Bénard problem is the nonzero flow field [Eqs. (3.24) and (3.25)] for any nonzero magnetic Rayleigh number. A similar phenomenon was observed at the onset of the Marangoni-Bénard convection over a heated substrate with grooves [15]. As in our system, no distinct transition from a pure conductive to a convective state occurred. Instead, the fluid convects for all nonzero values of the external magnetic driving force.

Therefore the base state is not the quiescent one any longer. In fact, Fig. 5 shows a structured flow field: it is given by a double vortex. (The material parameters $\rho_0=1.356\times10^3$ kg/m^3, $\alpha=4.5\times10^{-4}$ K^{-1}, $\eta=150\times10^{-3}$ kg/(m s), $\kappa=5\times10^{-8}$ m^2/s, and $K=35$ A/(m K) of APG 513A were used with $T_b=30\,^\circ$C and $T_t=20\,^\circ$C.) That means that for a symmetrical arrangement of bars not only does a nonzero flow field exist, but also it has the nonsimple structure of a double vortex. Considering the shape of a single vortex, it is stretched in the x direction due to the modulation with a long wavelength in order to fulfill $k\,d\ll1$. Thus the wavelength of the sinusoidal variation of the magnetic field strongly influences the x extension of the vortex. For too large wavelengths it is expected that the system will hardly form an elongated eddy which will stretch for several tens of layer thicknesses. In contrast, for rather small wavelengths of the modulation the system will "see" only a mean value,

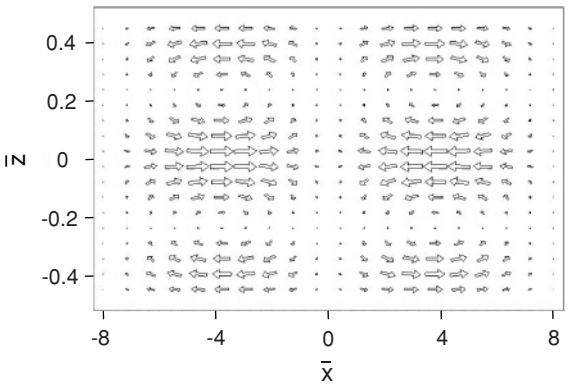

FIG. 5. Plot of the flow field for a scaled temperature difference of $\delta\bar{T}=1$ which gives together with the other material parameters (see text) $\mathrm{Ra}\simeq63.8$ and $\mathrm{Ra}_m\simeq82.1$.

obliterating the effect of a spatial variation. In which interval of intermediate wavelengths the vortex will match the length scale of the external excitation is a question to be answered in experiments.

In these a practical procedure to reach the base state would consist of two steps. First, a small temperature gradient is applied across the layer, which results in an undercritical Rayleigh number, e.g., only heat conduction is present. Second, the magnetic field is switched on and the convective base state will form.

C. Linear stability

To determine the stability of this base state, a linear stability analysis is performed. Since the components of the flow field of the base state can be expressed with the help of a stream function,

$$\Psi_b(\bar{x},\bar{z})=-\left[\sin(\bar{k}\bar{x})+\frac{E}{2}\sin(2\bar{k}\bar{x})\right]\times\mathrm{Ra}_m E(\mu_r-1)\frac{\bar{z}(4\bar{z}^2-1)^2\bar{k}^3}{1920\mu_r^2}, \quad (3.27)$$

i.e., $\mathbf{v}_b=(\partial\Psi_b/\partial\bar{z},0,-\partial\Psi_b/\partial\bar{x})$, small two-dimensional disturbances

$$\Psi_b\to\Psi_b+\Phi(\bar{x},\bar{z},\bar{t}), \quad (3.28)$$

$$T_b\to T_b+\Theta(\bar{x},\bar{z},\bar{t}), \quad (3.29)$$

expand the base state. With the introduction of Ψ_b, the governing equations are restricted to $O(\bar{k}^3)$ for the disturbances. With the ansatz [Eqs. (3.28) and (3.29)], the Navier-Stokes equation and the equation of heat conduction, respectively, have the form

$$0=\Delta^2\Phi-\mathrm{Ra}\frac{\partial\Theta}{\partial\bar{x}}, \quad (3.30)$$

$$0=-\Delta\Theta+\frac{\partial\Theta}{\partial\bar{t}}+\frac{\partial\Phi}{\partial\bar{x}}+\frac{\partial\Psi_b}{\partial\bar{z}}\frac{\partial\Theta}{\partial\bar{x}}. \quad (3.31)$$

After differentiating Eq. (3.31) with respect to $\bar{x}$ and using Eq. (3.30) to substitute $(\partial\Theta/\partial\bar{x})$, the final linear equation for $\Phi(\bar{x},\bar{z},\bar{t})$ is

$$\frac{\partial}{\partial\bar{t}}\Delta^2\Phi + \mathrm{Ra}\frac{\partial^2\Phi}{\partial^2\bar{x}} + \frac{\partial\Psi_\mathrm{b}}{\partial\bar{z}}\frac{\partial}{\partial\bar{x}}\Delta^2\Phi = \Delta^3\Phi \qquad (3.32)$$

under the condition that $\mathrm{Ra} \neq 0$ holds. To solve this equation, the separation ansatz for small disturbances

$$\Phi(\bar{x},\bar{z},\bar{t}) = e^{i\bar{q}\bar{x}}\cos(\pi\bar{z})e^{\bar{\sigma}\bar{t}}\sum_{l=-N}^{N} f_l\, e^{il\bar{k}\bar{x}} \qquad (3.33)$$

decomposed them as follows. The exponential function with the growth rate $\bar{\sigma}$ describes the exponential growth ($\bar{\sigma} > 0$) or decay ($\bar{\sigma} < 0$) of the disturbances. The term $\cos(\pi\bar{z})$ fulfills automatically the stress-free boundary conditions at the plates and approximates the exact z dependence which would require the entire sum $\sum_{m=1}^{N}\cos(m\pi\bar{z})$. With respect to $\bar{x}$ a Floquet ansatz is made which is typical for modulated problems [16], where $\bar{q}$ denotes the dimensionless wave number of the disturbances.

By inserting the ansatz (3.33) into Eq. (3.32), the appearing explicit dependence on z is eliminated by multiplying the resulting equation with $\cos(\pi\bar{z})$ and integrating over z from $-1/2$ to $1/2$. Arranging all terms which are proportional to $e^{il\bar{k}\bar{x}}$, an eigenvalue problem of the sort

$$\bar{\sigma}\mathbf{f} = \mathcal{A}\mathbf{f}, \quad \mathbf{f} = (f_{-\mathrm{N}}, \ldots, f_{\mathrm{N}}), \qquad (3.34)$$

appears, where $\mathcal{A}$ is a band matrix with the elements

$$\mathcal{A}_{\mathrm{l,l}} = \frac{\mathrm{Ra}(\bar{q}+\bar{k}l)^2}{[(\bar{q}+\bar{k}l)^2+\pi^2]} - (\bar{q}+\bar{k}l)^2 - \pi^2, \qquad (3.35)$$

$$\mathcal{A}_{\mathrm{l,l}\pm1} = \mp\frac{\tilde{\mathrm{P}}[\bar{q}+\bar{k}(l\pm1)]\{[\bar{q}+\bar{k}(l\pm1)]^2+\pi^2\}}{2[(\bar{q}+l\bar{k})^2+\pi^2]^2}, \qquad (3.36)$$

$$\mathcal{A}_{\mathrm{l,l}\pm2} = \mp\frac{\tilde{\mathrm{P}}[\bar{q}+\bar{k}(l\pm2)]\{[\bar{q}+\bar{k}(l\pm2)]^2+\pi^2\}}{2[(\bar{q}+l\bar{k})^2+\pi^2]^2}, \qquad (3.37)$$

with

$$\tilde{\mathrm{P}} = \mathrm{Ra}_m\frac{(\mu_r-1)E(15-\pi^2)\bar{k}^3}{240\mu_r^2\pi^4} \qquad (3.38)$$

containing the magnetic force. By determining the marginal stability ($\bar{\sigma} = 0$), the threshold of stability for the base state can be determined. The results of these calculations will be presented in the next section.

IV. RESULTS AND DISCUSSION

As a step of validation, the threshold for vanishing magnetic force, $\mathrm{Ra}_m = 0$, is determined. Solving the eigenvalue problem (3.34) with this constraint, a minimal threshold of

$$\mathrm{Ra}_c(\mathrm{Ra}_m = 0, \bar{q}_{\mathrm{c},0}) = \mathrm{Ra}_{c,0} = \frac{27}{4}\pi^4 \qquad (4.1)$$

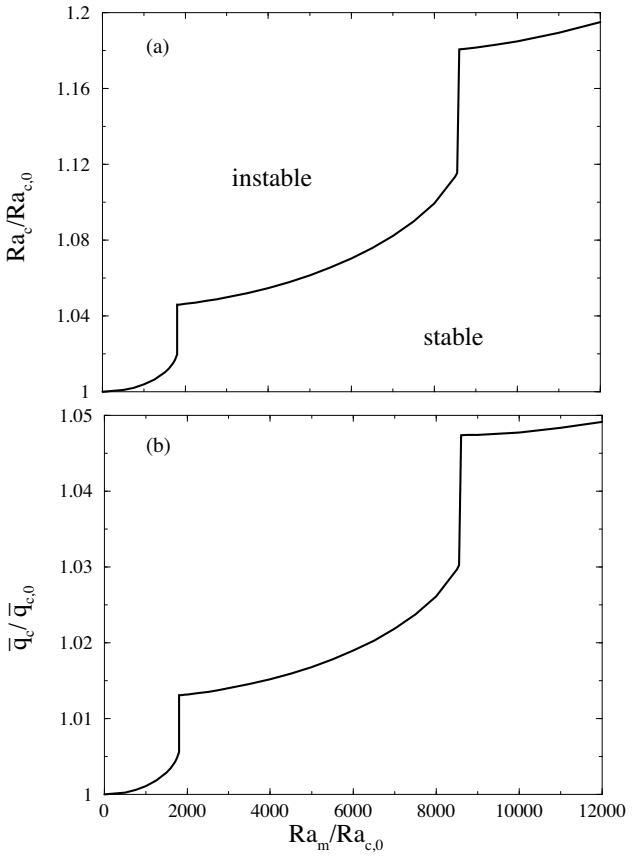

FIG. 6. Plots of the critical Rayleigh number Ra_c (a) and the critical wave number $\bar{q}_\mathrm{c}$ (b) scaled with the corresponding values for a purely thermal driving mode against the strength of the magnetic driving force. By increasing Ra_m, the critical Rayleigh number increases slightly. That rise is accompanied by an increase of the critical wave number. For the sudden jumps in both quantities, see text.

at

$$\bar{q}_\mathrm{c}\,(\mathrm{Ra}_m = 0) = \bar{q}_{\mathrm{c},0} = \frac{\pi}{\sqrt{2}} \qquad (4.2)$$

results, which is known from the classical Rayleigh-Bénard problem for stress-free boundary conditions [2].

By minimizing Ra with respect to $\bar{q}$ at a given nonzero value of Ra_m, the threshold between the stable and unstable region for the base state is determined. The critical Rayleigh number Ra_c and the critical wave numbers $\bar{q}_\mathrm{c}$, respectively, scaled with the corresponding values for a purely thermal driving mode, are plotted in Fig. 6. The stability chart shows that with increasing magnetic Rayleigh number Ra_m, the critical Rayleigh number Ra_c increased slightly. That increase is accompanied by an increase of the critical wave number $\bar{q}_\mathrm{c}$. A larger wave number means more convection rolls per length, which requires more energy which is reflected by the growing critical Rayleigh number which on its part is equivalent to a stronger external driving force.

The behavior of both quantities is different from that in a Rayleigh-Bénard system, where the temperature of the bottom plate is spatially modulated [16]. There the threshold shows a slight decrease at an almost constant critical wave number.

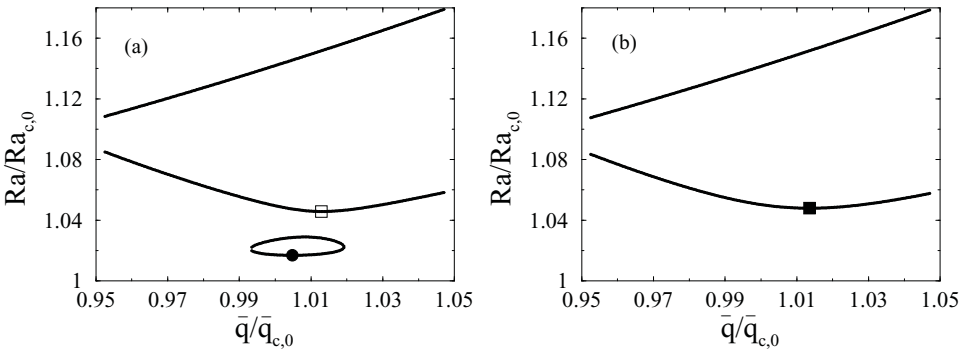

FIG. 7. Plot of the solution $\bar{\sigma} = 0$ (solid lines) in the scaled $\bar{q}$-Ra plane for two different strengths of magnetic force with $\mathrm{Ra}_m/\mathrm{Ra}_{c,0} = 1750$ (a) and $\mathrm{Ra}_m/\mathrm{Ra}_{c,0} = 2500$ (b). The filled (empty) symbols denote the lowest (second lowest) local minimum.

Compared to that, the excitation by a spatially modulated field offers apparently a greater freedom for the system to choose its wave number. As already described in [16], the neutral curve $\mathrm{Ra}(\bar{q})$, where the growth rate is zero, possesses several local minima that are separated by $\bar{k}$. No absolute minimum with respect to $\bar{q}$ could be determined here despite the selection of $N = 11$ in Eq. (3.33). For this choice, the numerical accuracy is such that no difference between consecutive local minima up to $O(10^{-8})$ could be found with $\mathrm{Ra}_c \sim O(10^3)$.

The sudden jumps in both critical quantities are the most remarkable property of the stability curve in Fig. 6. To understand this behavior, one has to envision that the neutral curve, i.e., $\bar{\sigma} = 0$, has not a unique solution at a fixed value of $\bar{q}$ as the two examples for $\mathrm{Ra}_m/\mathrm{Ra}_{c,0} = 1750$ and $\mathrm{Ra}_m/\mathrm{Ra}_{c,0} = 2500$ in Fig. 7 show. Depending on the magnetic driving force, the solution forms tongues and islands, as it is known from the Faraday instability [17,18]. The similarity stems from the fact that the systems are periodically modulated: in one case with respect to time, in the other with respect to space.

For the lower value of the magnetic force, see Fig. 7(a), a lowest minimum (filled circle) at an island and a second lowest (empty square) at a tongue exist. As the magnetic Rayleigh number increases, the island part of the neutral curve shrinks until it disappears completely. That is shown in Fig. 7(b) for a second value of the magnetic Rayleigh number. At that condition the second lowest minimum from Fig. 7(a) becomes the lowest one in Fig. 7(b) (filled square) and the stability curves make a jump.

That is the reason for the drastic changes in the stability chart at some particular values of the magnetic Rayleigh number, where the first jump is shown in a zoom of Fig. 6 in Fig. 8. The lowest and second lowest minimum at selected values of the scaled magnetic Rayleigh number are again indicated by the corresponding filled and empty symbols, respectively. The solid line shows the threshold between stability and instability. The black long-dashed line is a guide for the eye for the second lowest minimum before the first jump of Ra_c. A similar behavior with less pronounced jumps for a critical quantity with respect to the onset of patterns was measured for the Faraday instability by Douady [19].

For a better understanding of the diverging increase of Ra_c close to the first jump, an analytical approach is chosen. For that purpose it is assumed that the critical wave number is equal to the one without a magnetic force, $\bar{q}_c = \bar{q}_{c,0}$ [the deviation is less than 1.5% according to Fig. 6(b)], and an approximation by selecting $N = 1$ is made. The eigenvalue problem (3.34) reduces now to a cubic equation for Ra which can be solved analytically. Exploiting that $\bar{k}/\pi$ is small compared to 1, the critical Rayleigh number is given by

$$\mathrm{Ra}_c = -12\pi\bar{k}^2\sqrt{1-\frac{E^2+8}{9830400}\tilde{A}} \times \cos\left\{\frac{1}{3}\arccos\left[\frac{1+\frac{E^2-4}{3276800}\tilde{A}}{\left(1-\frac{E^2+8}{9830400}\tilde{A}\right)^{3/2}}\right]\right\} + \frac{27\pi^4}{4}\frac{\left(1-\frac{20}{9}\frac{\bar{k}^2}{\pi^2}+\frac{76}{81}\frac{\bar{k}^4}{\pi^4}+\frac{160}{81}\frac{\bar{k}^6}{\pi^6}+\frac{32}{81}\frac{\bar{k}^8}{\pi^8}\right)}{\left(1-2\frac{\bar{k}^2}{\pi^2}\right)^2}, \tag{4.3}$$

with

$$\tilde{A} = \mathrm{Ra}_m^2\frac{(\mu_r-1)^2(15-\pi^2)^2E^2\bar{k}^2}{\mu_r^4\pi^6}. \tag{4.4}$$

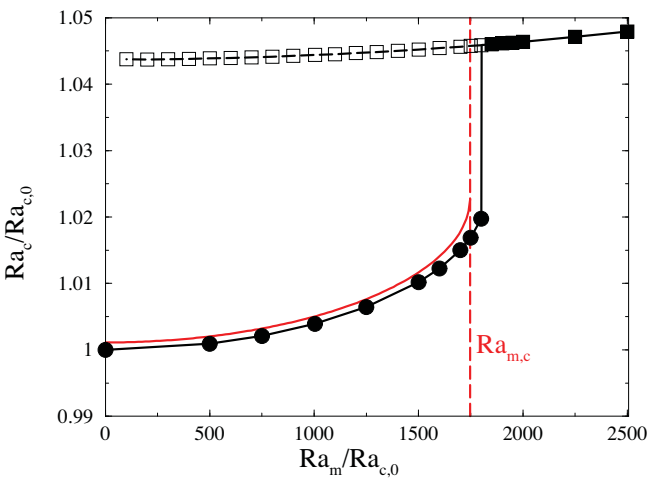

FIG. 8. (Color online) Plot of the scaled critical Rayleigh number (black solid line) vs the scaled strength of the magnetic driving force. The lowest and second lowest minimum of the neutral curve is indicated by the filled and empty symbols, respectively. The black long-dashed line is a guide for the eye for the second lowest minimum before the first jump of $\mathrm{Ra}_c/\mathrm{Ra}_{c,0}$. The red (gray) solid and long-dashed lines indicate analytical results with the assumptions $\bar{q}_c = \bar{q}_{c,0}$ and $N = 1$ in Eq. (3.33), see text.

The solid red (gray) line in Fig. 8 shows the numerical evaluation of the analytical result (4.3). Despite the approximations, the data of the full eigenvalue problem are nicely fitted including the divergence of the threshold near a critical value of the magnetic Rayleigh number. That number can be approximately determined, too, by the condition that the absolute value of the argument of the arccos function has to be smaller than 1. The limit $[\cdots] = 1$ in Eq. (4.3) yields

$$\mathrm{Ra}_{m,c} = \frac{3840\sqrt{2}\pi^3\mu_r^2}{E\bar{k}(\mu_r - 1)(15 - \pi^2)} \times \sqrt{\frac{E^2(20 - E^2) + 8\left[1 + \sqrt{(1 - E^2)^3}\right]}{(E^2 + 8)^3}}, \tag{4.5}$$

which is indicated by the vertical red (long-dashed) line in Fig. 8. Thus the lowest order in the Floquet ansatz generates analytical results for both Ra and Ra_m which shed light on the deeper reasons for the behavior of the threshold.

Figures 6 and 8 reveal that for small changes of the critical Rayleigh number of about a few percent, the scaled magnetic Rayleigh number has to be large. Nevertheless it is expected that the flow field is well structured and not turbulent. Such a behavior was detected by Yamaguchi *et al.* [20] with their experimental and numerical investigation of convectional phenomena in a similar setup. For a scaled Rayleigh number of 1.4 and a scaled magnetic Rayleigh number of 3×10^5, only "weak flow roll" occurred, as the authors noted [20]. A second aspect of the large magnetic Rayleigh numbers is their experimental feasibility. With an upper bond of $K_{\max} = 50\ \mathrm{A/(m\,K)}$ and $\delta T_{\max} = 65\ \mathrm{K}$ [7], one can achieve for a 2 mm layer of APG 513A a maximal scaled magnetic Rayleigh number of $(\mathrm{Ra}_m/Ra_{c,0})_{\max} \simeq 10$. That is too small to explore the wide range of the stability threshold plotted in Fig. 8.

To extend the testing area, an alternative approach comes into play. That approach is a combination of the inner gradient of the magnetic field, reflected by the pyromagnetic coefficient K, and an external gradient, ∇H_{ext}, which results in a different definition of the magnetic Rayleigh number,

$$\mathrm{Ra}_m = \frac{\mu_0 K \delta T \nabla H_{\mathrm{ext}} d^3}{\kappa\,\eta}. \tag{4.6}$$

The exploitation of such a concept for thermomagnetic convection was already shown in [21]. To reach a scaled magnetic Rayleigh number of 2000, necessary to cover the first jump in the stability curve [see Figs. 6(a) and 8], an external field gradient of $\nabla H_{\mathrm{ext}} = 3 \times 10^8\ \mathrm{A/m^2}$ is needed. The realization of such a gradient is the subject of current research. With strong external gradients of the applied magnetic field, the presented base flow will experience a modification whose extent will be examined in a future study.

V. CONCLUSION

A detailed analysis of the thermomagnetic convection in a horizontal layer of magnetic fluid subjected to a spatially and symmetrical modulated magnetic field is presented. For any nonzero magnetic field the base state is a convective one in contrast to the classical Rayleigh-Bénard system which is purely thermally driven. The nonzero flow field of the base state is formed by a double vortex which reflects the symmetrical modulation from above and beneath the layer of magnetic fluid. The linear stability analysis reveals that the threshold for the stability of the base state increases with increasing magnetic driving force. In the lowest order of the chosen Floquet ansatz it is possible to derive an analytical expression for the threshold showing the characteristic feature of sudden jumps of the threshold at particular values of the magnetic driving force.

The easy and modular variation of the external modulation of the magnetic field triggers new tasks from the theoretical point of view. It would be of high interest to determine the base state and its stability if only one iron bar is used, if two iron bars of the same wavelength but with a phase shift are employed, or if two iron bars with different wavelengths are applied. For all types of modulations, the influence of its wavelength on the size of the vortex of the base flow is of particular interest, because this influence competes with the geometrical constraints which determine also the size of convection patterns as known from the classical Rayleigh-Bénard setup. These questions are deferred to a forthcoming publication, as well as objectives which are of importance from an experimental point of view. These objectives comprise, for instance, the realization of such systems, the measurement of the stability threshold, and particularly the detection of a convective base state formed by a double vortex.

ACKNOWLEDGMENTS

The authors thank Harald Engler for providing the material data of APG 513A.

[1] M. C. Cross and P. C. Hohenberg, Rev. Mod. Phys. **65**, 851 (1993).
[2] S. Chandrasekhar, *Hydrodynamics and Hydrodynamic Stability* (Dover, New York, 1981).
[3] F. Hébert, R. Hufschmid, J. Scheel, and G. Ahlers, Phys. Rev. E **81**, 046318 (2010).
[4] J. L. Rogers, M. F. Schatz, J. L. Bougie, and J. B. Swift, Phys. Rev. Lett. **84**, 87 (2000).
[5] S. W. Morris, E. Bodenschatz, D. S. Cannell, and G. Ahlers, Phys. Rev. Lett. **71**, 2026 (1993).
[6] G. Ahlers, P. C. Hohenberg, and M. Lücke, Phys. Rev. A **32**, 3519 (1985).
[7] H. Engler and S. Odenbach, J. Phys. Condens. Matter **20**, 204135 (2008).
[8] L. Schwab, U. Hildebrandt, and K. Stierstadt, J. Magn. Magn. Mater. **39**, 113 (1983).
[9] L. Schwab and K. Stierstadt, J. Magn. Magn. Mater. **65**, 315 (1987).
[10] L. Schwab, J. Magn. Magn. Mater. **85**, 199 (1990).
[11] L. Schwab, Ph.D. thesis, Tech. Univ. München, 1989.

[12] A. Recktenwald and M. Lücke, J. Magn. Magn. Mater. **188**, 326 (1998).
[13] S. A. Suslov, Phys. Fluids **20**, 084101 (2008).
[14] P. N. Kaloni and J. X. Lou, Phys. Rev. E **70**, 026313 (2004).
[15] A. D. Stroock, R. F. Ismagilov, H. Stone, and G. M. Whitesides, Langmuir **19**, 4358 (2003).
[16] R. Schmitz and W. Zimmermann, Phys. Rev. E **53**, 5993 (1996).
[17] S. Kumar, Phys. Fluids **11**, 1970 (1999).
[18] H. W. Müller and W. Zimmermann, Europhys. Lett. **45**, 169 (1999).
[19] S. Douady, J. Fluid Mech. **221**, 383 (1990).
[20] H. Yamaguchi, X. Niu, X. Zhang, and K. Yoshikawa, J. Magn. Magn. Mater. **321**, 3665 (2009).
[21] S. Odenbach, J. Magn. Magn. Mater. **149**, 155 (1995).